Supplementary Material (ESI) for Journal of Materials Chemistry

Supporting information:

Macro-/microporous MOF composite beads

Laura D. O'Neill, Haifei Zhang and Darren Bradshaw*

University of Liverpool, UK. Email: deg5y@liv.ac.uk

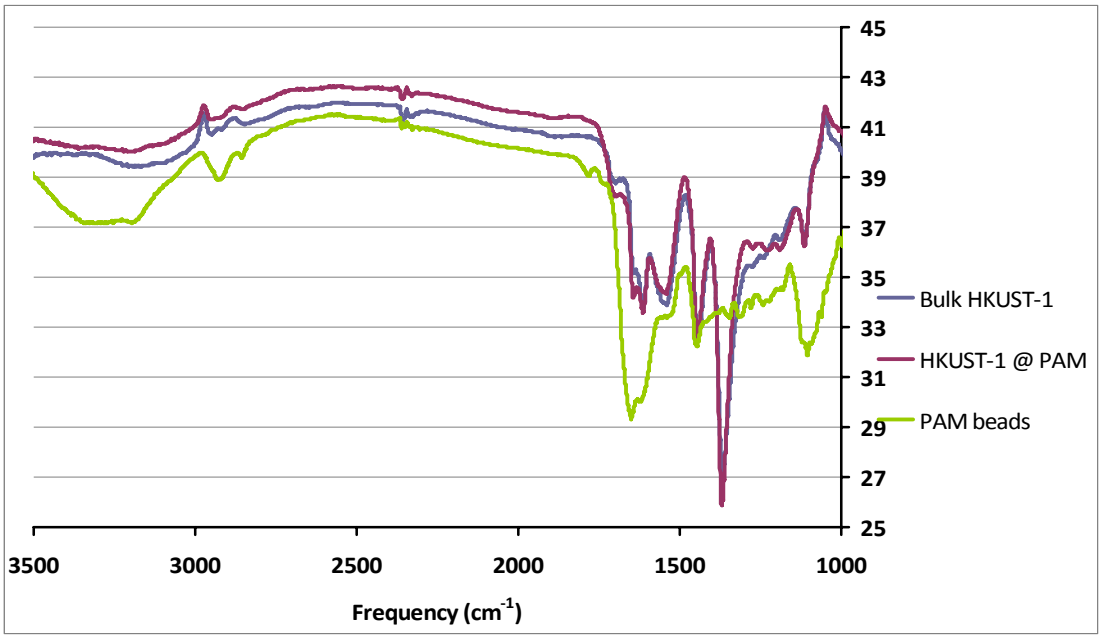

Figure S1 FTIR data collected in the range 3500 – 1000 cm^{-1} using a JASCO FT/IR-4100 spectrometer in the solid-state, confirm the presence of HKUST-1 in the original (solvothermal) HKUST-1@PAM_1.0 composite material. PAM 1652 cm^{-1} (C=O, 1° amide), 1632 cm^{-1} (N-H bend); HKUST-1 1645, 1616, 1553, 1453 cm^{-1} (C=O symm and asymm, Ar-C=C), 1371 (C-O); composite 1645, 1617, 1561, 1455 cm^{-1} (C=O symm and asymm, Ar- C=C), 1372 (C-O). The composite spectrum is dominated by HKUST-1 in the region 1700 – 1400 cm^{-1}, obscuring the peaks attributable to the primary amide of the PAM.

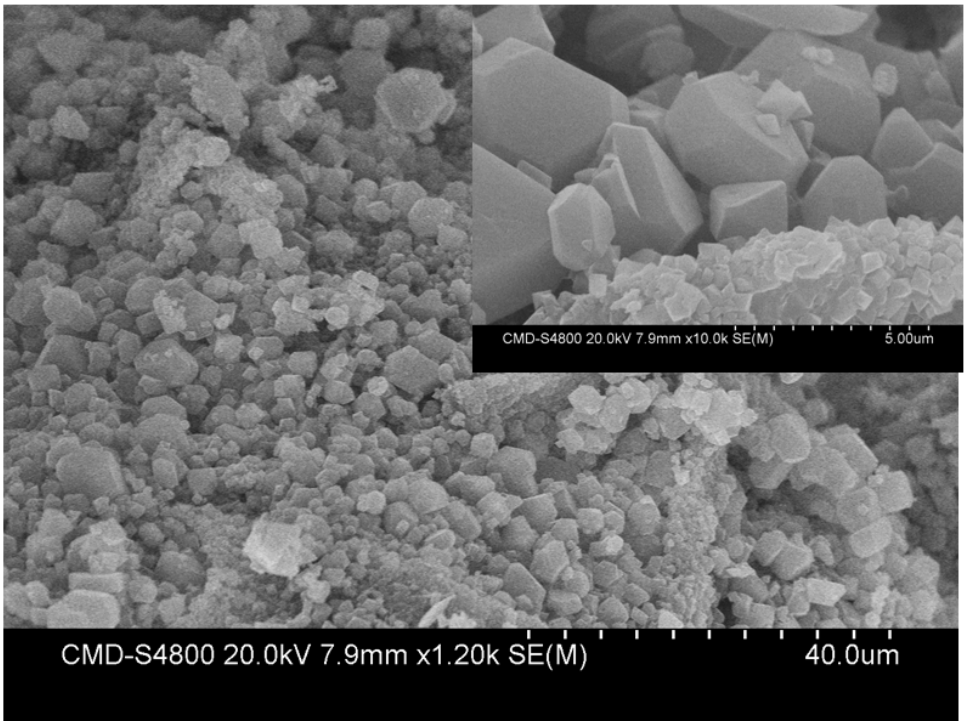

Figure S2 SEM images of HKUST-1@PAM_0.5 (scale of inset is 5 μm) prepared by adding PAM beads to a solvothermal HKUST-1 synthesis at 0.5 x the original concentration of 0.7M Cu and 1.6M BTC.

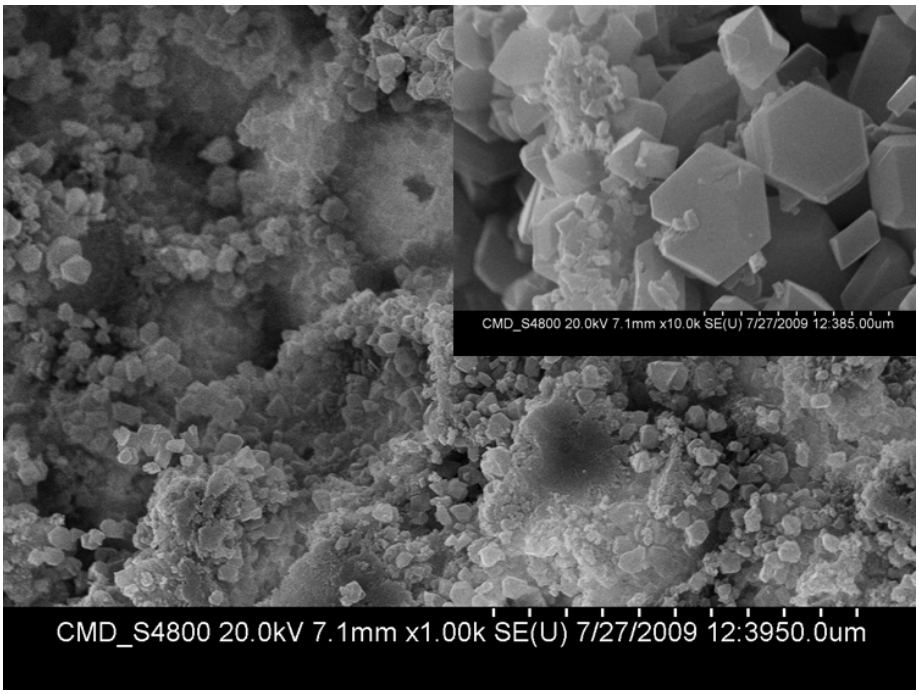

Figure S3 SEM images of HKUST-1@PAM_0.2 (scale of inset is 5 μm) prepared by adding PAM beads to a solvothermal HKUST-1 synthesis at 0.2 x the original concentration of 0.7M Cu and 1.6M BTC.

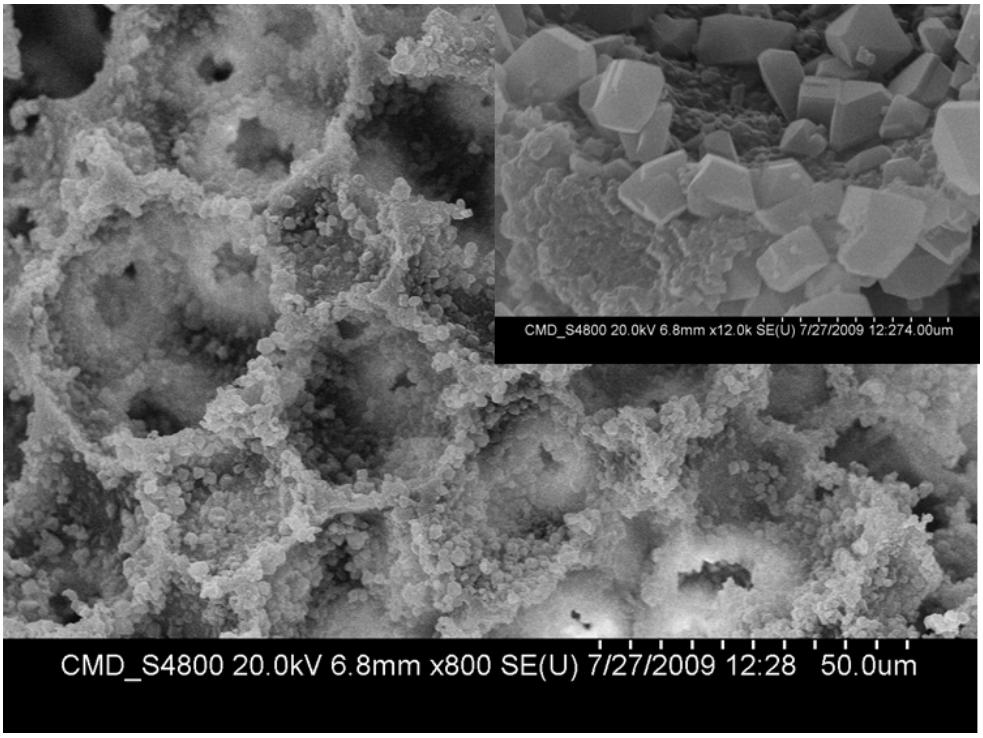

Figure S4 SEM images of HKUST-1@PAM_0.1 (scale of inset is 4 μm) prepared by adding PAM beads to a solvothermal HKUST-1 synthesis at 0.1 x the original concentration of 0.7M Cu and 1.6M BTC.

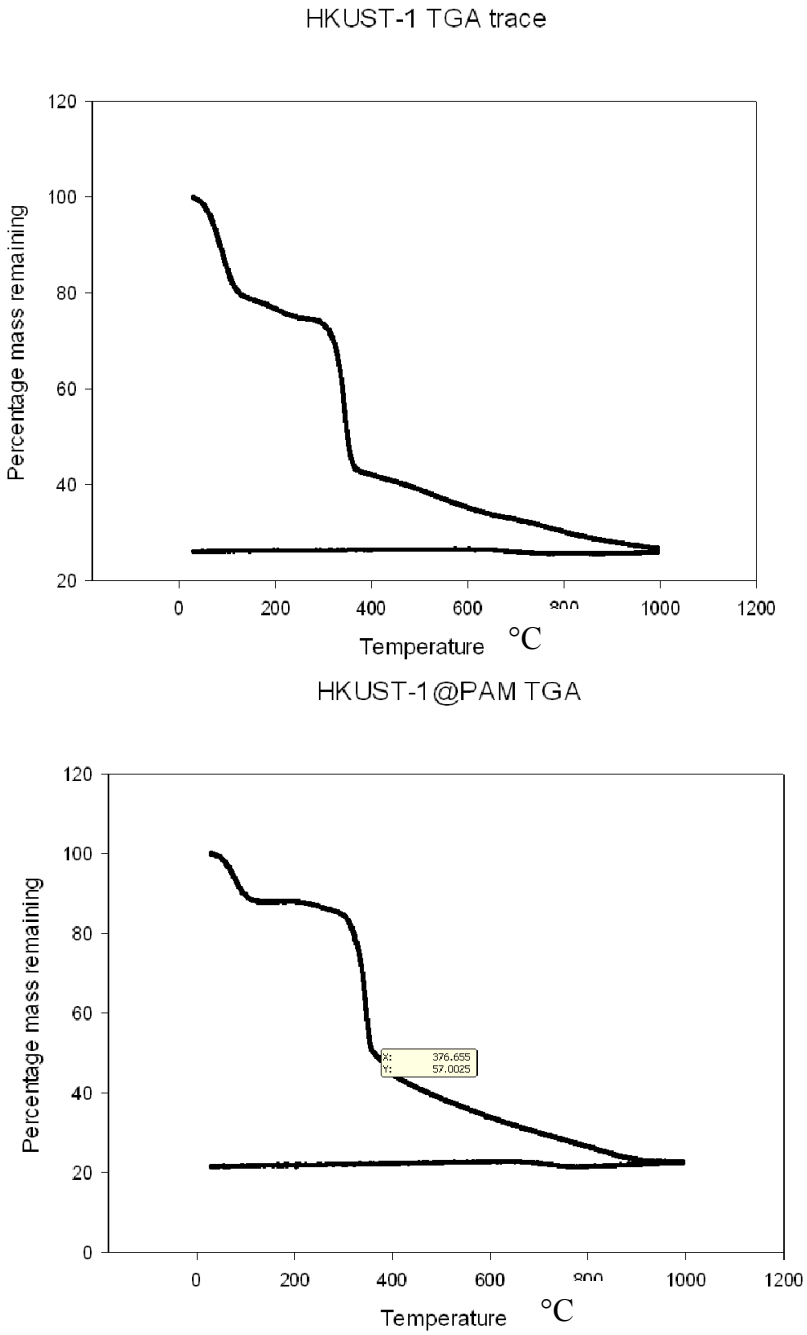

Figure S5 TGA data of bulk HKUST-1 (top) and HKUST-1@PAM_1.0 composite prepared solvothermally using a reaction concentration of 0.75M metal and 0.16M BTC. Mass loss for the MOF guest molecules and metal-bound H_2O molecules up to 300°C is 25% for bulk HKUST-1 and 12% for the composite (*viz*. 60% of that observed for the bulk phase). Above this temperature, the mass loss corresponding to the thermal decomposition of organics is 47% for HKUST-1 and 65% for the composite; the composite thus contains 38% more organic material than pure HKUST-1. This confirms the 3:2 MOF:PAM stoichiometry for this material determined from the N_2 sorption isotherms. The amount of Cu present (4.512 mg, calculated from the remaining CuO after composite combustion) is used to calculate the amount of MOF in the composite from the mass of desolvated $[Cu_3(BTC)_2]$@PAM (7.305 mg) observed at the end of the first plateau (300°C), giving a stoichiometry of HKUST-1:PAM_1.0 of 0.62:0.38 The analytical composition of the bulk HKUST-1 recovered from the reaction is $[Cu_3(BTC)_2(H_2O)_3] \cdot 8(H_2O)$.

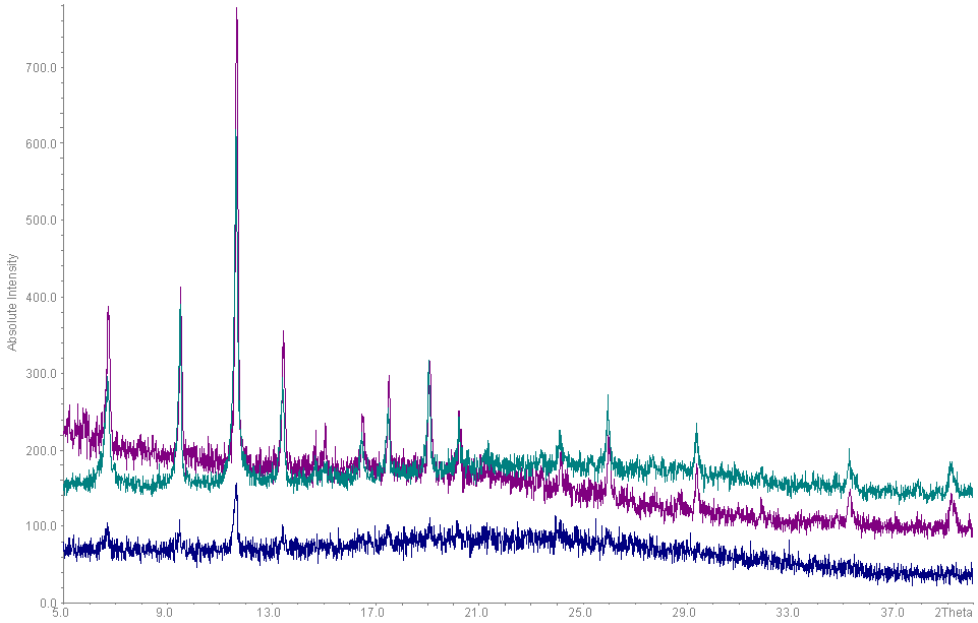

Figure S6 Powder X-ray diffraction data of the HKUST-1@PAM composites (HKUST-1@PAM_0.1, blue; HKUST-1@PAM_0.2, purple; HKUST-1@PAM_0.5, green) prepared solvothermally, collected in transmission mode using monochromated Cu-Kα1 radiation. Samples were ground and sealed in 0.5 mm glass capillaries.

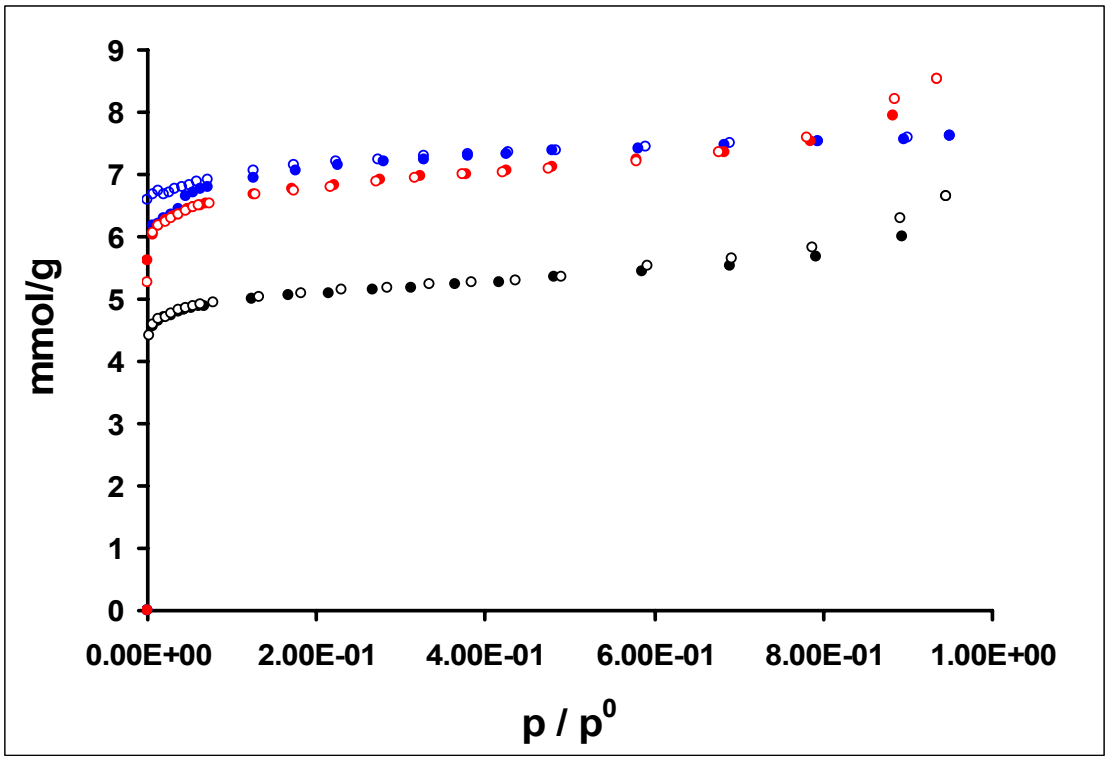

Figure S7 Variability of HKUST-1@PAM_0.5 composites prepared from solvothermal syntheses using different batches of PAM beads. Nitrogen uptakes at 77K and p/p^0 = 0.8 are 5.67 (black), 7.53 (blue) and 7.52 (red) mmol/g. The upturn of the black and red isotherms at high relative pressures, and the slight hysteresis through this feature on desorption, may indicate a small degree of inter-crystallite mesoporosity in the composites.

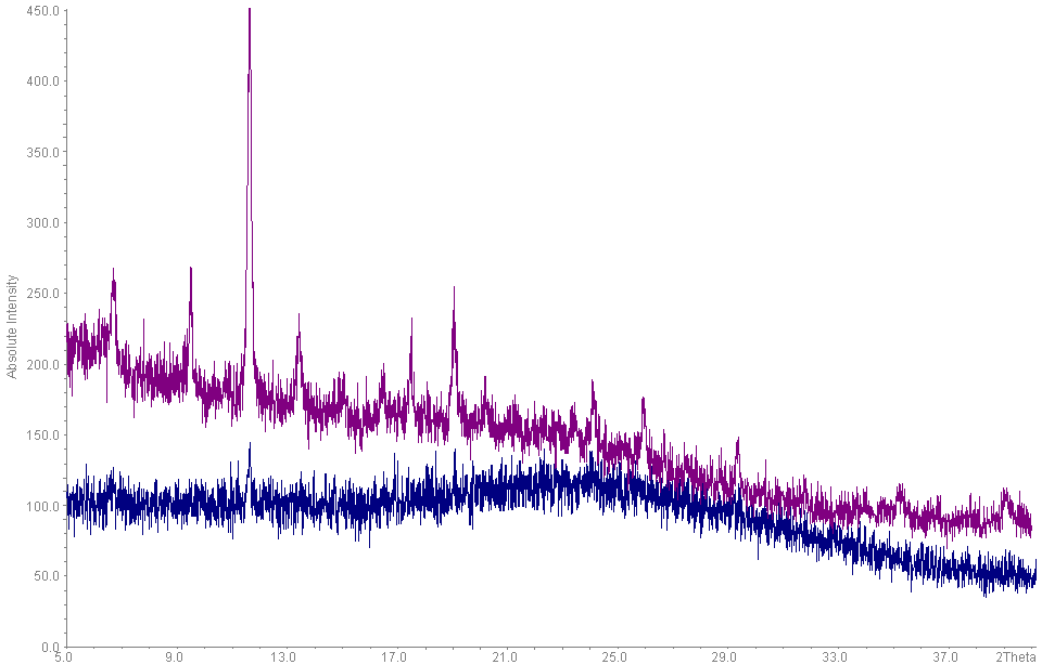

Figure S8 Powder X-ray diffraction data of the HKUST-1@PAM composites prepared solvothermally from the Cu^{2+}@PAM precursor beads ($Cu(NO_3)_2$, blue; $Cu(OAc)_2$, purple) and the BTC ligand, collected in transmission mode using monochromated Cu-Kα1 radiation. Samples were ground and sealed in 0.5 mm glass capillaries.

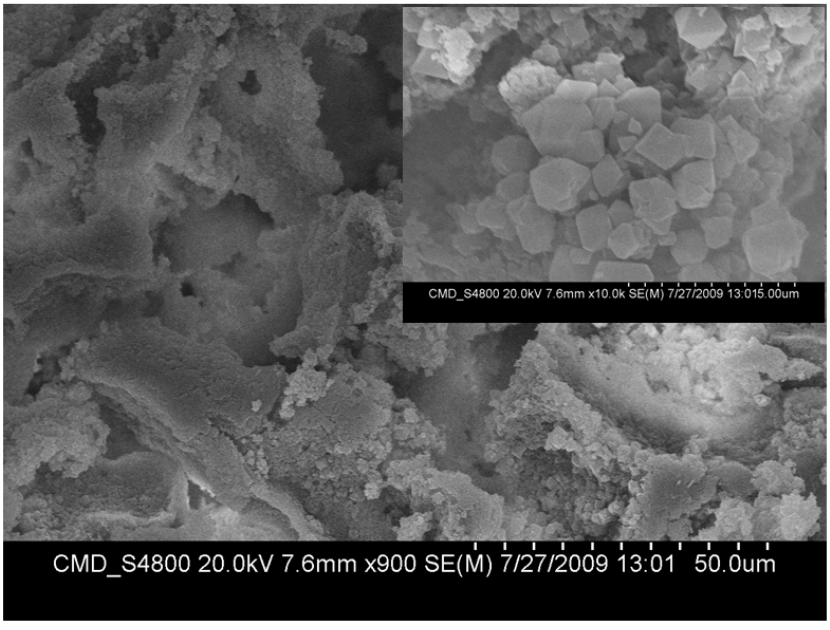

Figure S9 SEM images of HKUST-1@PAM_Ac composite (scale of inset is 5 μm)

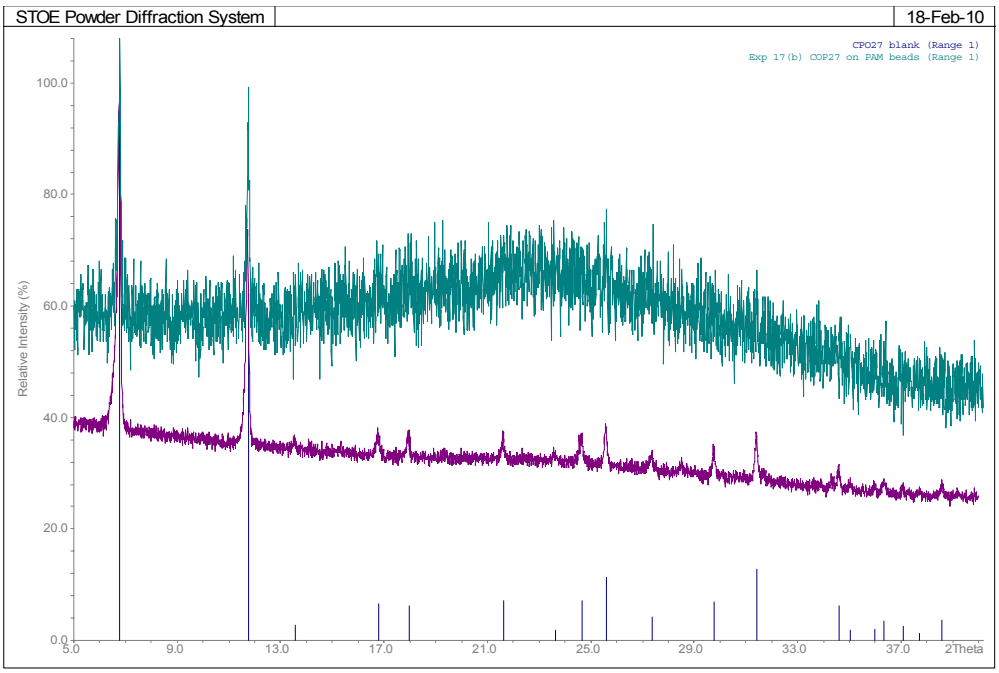

Figure S10 PXRD data of the solvothermally prepared CPO-27@PAM composite (green), recovered bulk CPO-27 (purple) and the indexed peak positions for the bulk phase (blue lines). The composite has a high background and a poor signal-to-noise ratio, but it is clear that the most intense reflections from the MOF are present. These data were collected in transmission mode using monochromated Cu-Kα1 radiation.

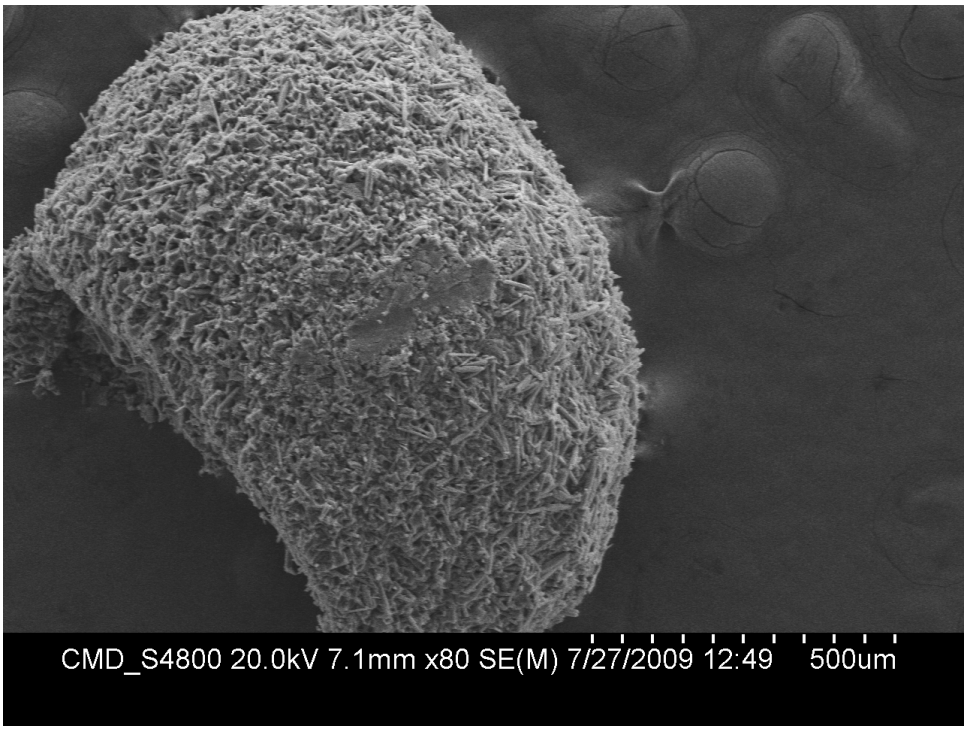

Figure S11. Exterior of a CPO-27@PAM composite bead clearly showing the crystal growth on the surface.

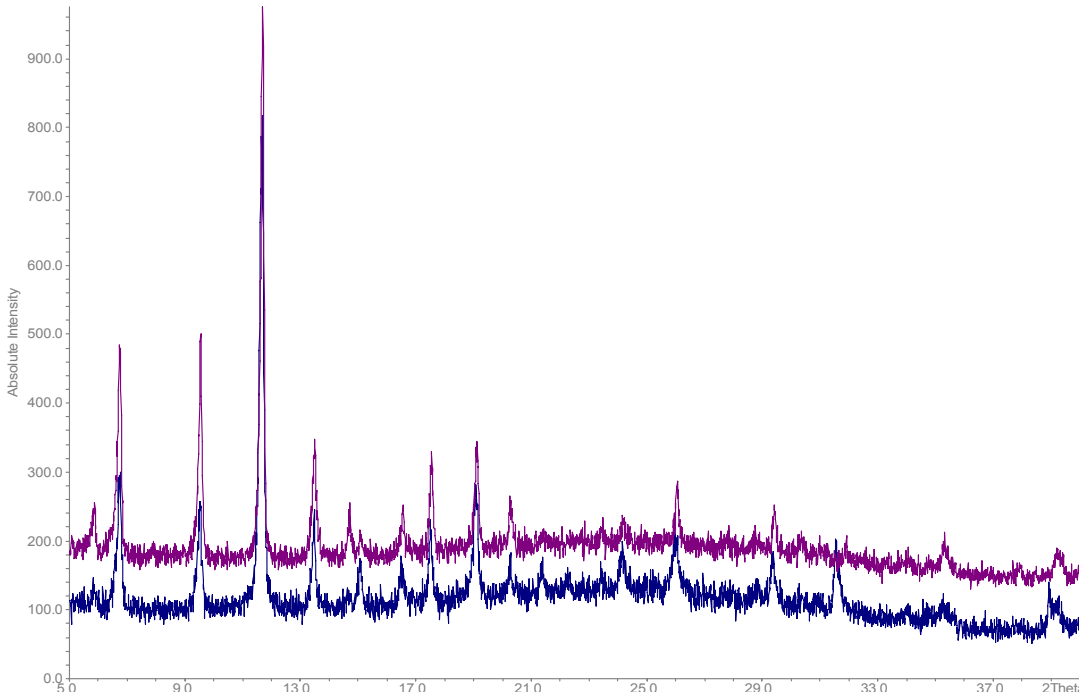

Figure S12 Powder X-ray diffraction data of the as-made HKUST-1@PAM_0.5 composite (purple) and after mechanically stirring in EtOH for 24 hrs (blue). These data were collected in transmission mode using monochromated Cu-Kα1 radiation.

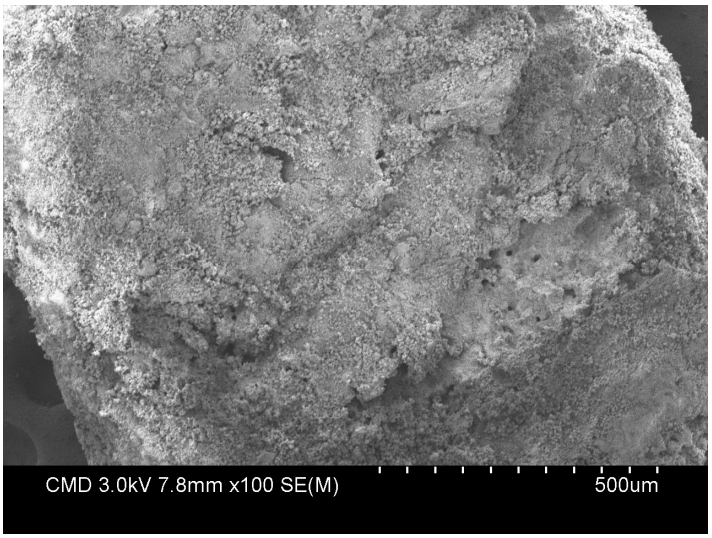

Figure S13. Close-up SEM image of a HKUST-1@PAM_0.5 composite bead after mechanically stirring in EtOH overnight.

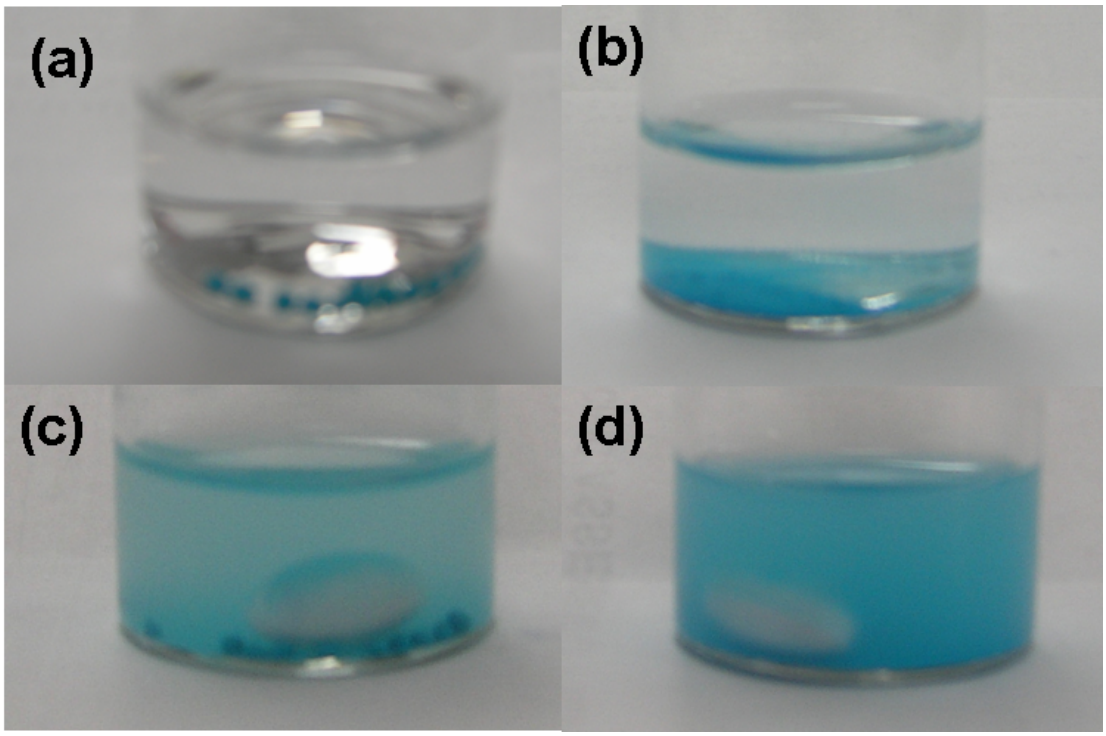

Figure S14. Digital images of HKUST-1@PAM composite beads (a, c) and bulk HKUST-1 (b, d) before (a, b) and after 30 mins standing (c, d) after 4 hours mechanical stirring with a 10 mm teflon-coated magnetic stirring bar in EtOH at 250 rpm. Images a and c clearly show that the composite beads remain intact after this treatment, although the solvent does take on a slight turbidity most likely as a result of MOF erosion from the exterior surface of the beads. The bulk MOF phase in image d took several hours to fully settle.

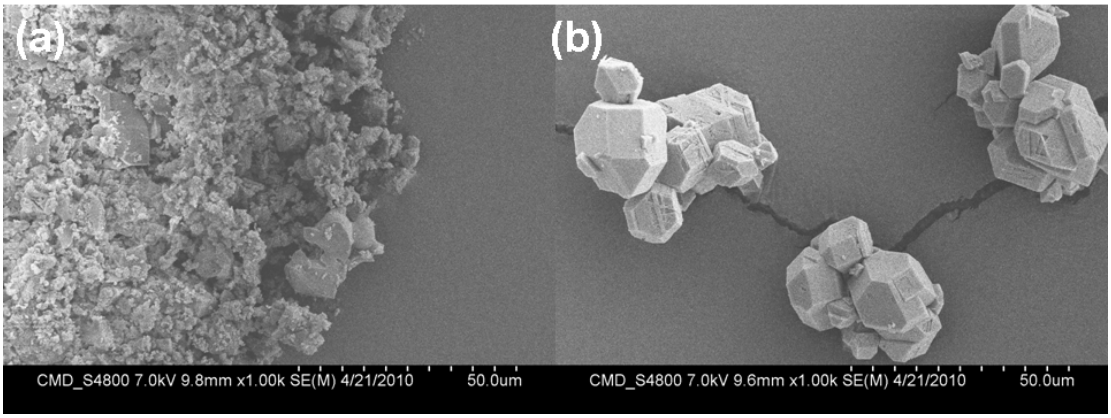

Figure S15. SEM images of bulk HKUST-1 after (a), and before (b), 4 hours mechanical stirring in EtOH. (For further detail of the stirring conditions see **S14** figure caption.) The images clearly show significant sample degradation after this process with many of the HKUST-1 crystals being eroded into a microcrystalline powder, consistent with the several hours taken for the sample to settle after stirring was stopped (**S14**, d).

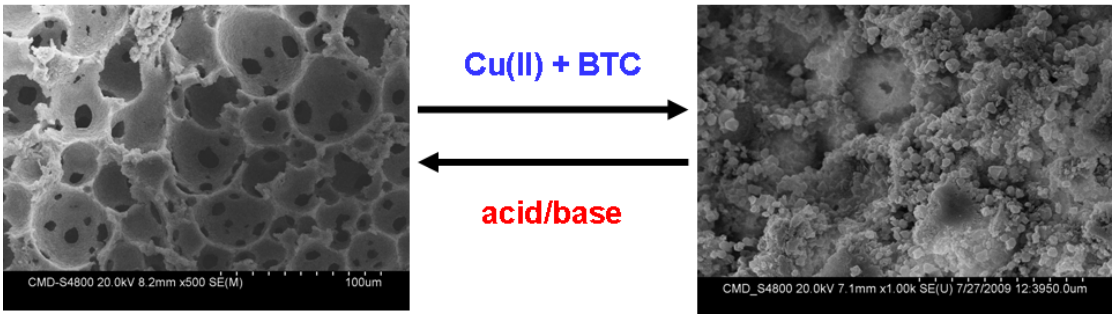

Figure S16 Reversibility of the HKUST-1@PAM composite reaction. The MOF crystallites are easily removed from the composite (right) to regenerate the intact macroporous PAM bead (left) by dissolving the MOF components in mild aqueous acid and base. In this case, the BTC ligand was first removed as a soluble tri-sodium salt, followed by treatment with HCl to remove residual Cu^{2+} as $[CuCl_4]^{2-}$.

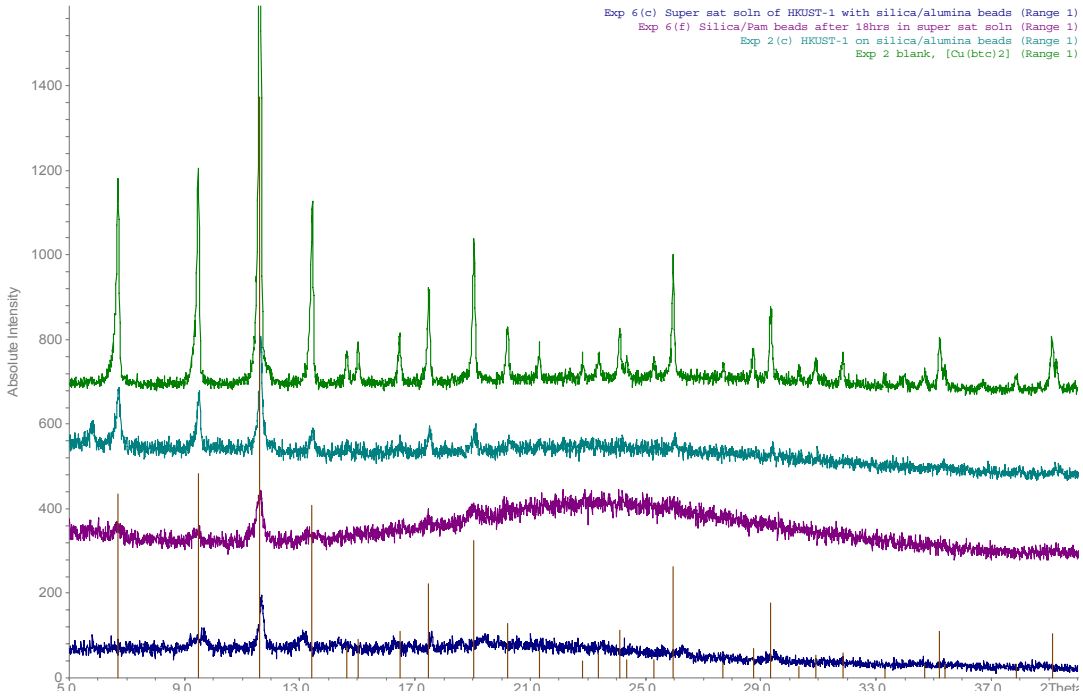

Figure S17. PXRD data of the HKUST-1@oxide composites. Pure bulk HKUST-1 (green), solvothermal HKUST-1@SiO_2-Al_2O_3 (light green), HKUST-1@SiO_2-PAM (purple) and HKUST-1@SiO_2-Al_2O_3 (blue) after 18 hrs in HKUST-1 mother solutions. The indexed peak positions for the bulk HKUST-1 are shown for information. These data were collected in transmission mode using monochromated Cu-Kα1 radiation.

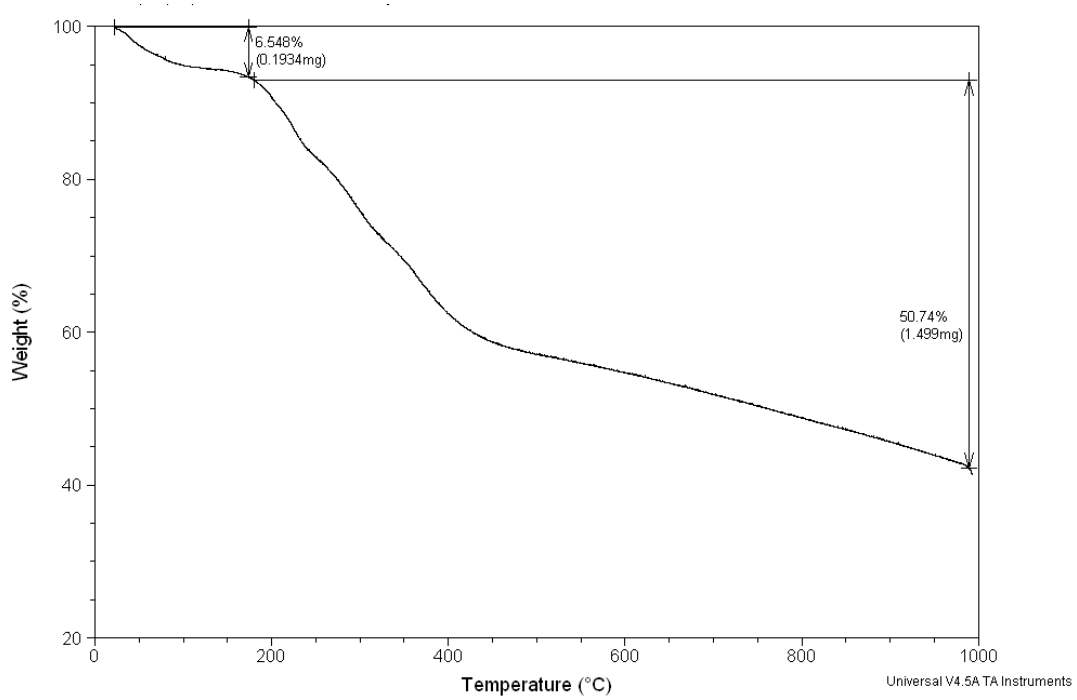

Figure S18. TGA data of HKUST-1@SiO_2-PAM composite beads prepared by immersing the SiO_2-PAM beads into a HKUST-1 mother solution for 8 days. The mass loss profile is less well-defined than in the case of HKUST-1@PAM, and it is not so clear where the organic components begin to degrade; however, carefully controlled mass loss data at 150°C under vacuum prior to isotherm measurement show a loss of 18% for MOF guests and other included species. From this point (T = 250°C) on the above TGA trace corresponding to a nominal composition of $[Cu_3(btc)_2]$@SiO_2-PAM, we can calculate that the ternary composite contains approximately 12% MOF from the remaining SiO_2 and CuO after combustion at 1000°C. (The SiO_2 content of the SiO_2-PAM beads was previously determined to be 46% oxide from TGA analysis of the as-made beads following a similar method)

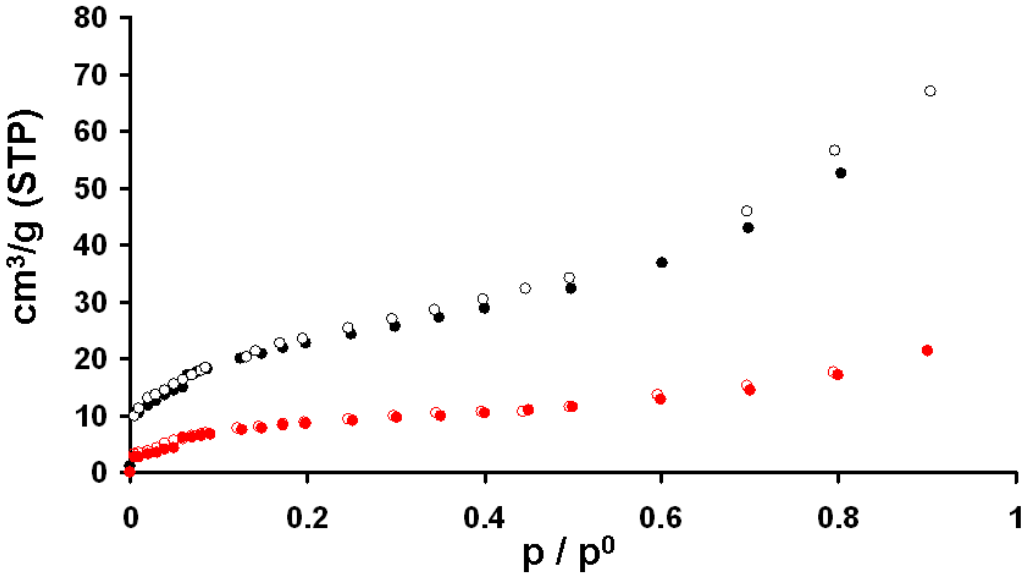

Figure S19. Nitrogen sorption isotherms of HKUST-1@SiO_2-PAM ternary composite beads (black) and as-made SiO_2-PAM (red) collected at 77K (closed circles, adsorption; open circles, desorption).